Nanoscale Advances

ROYAL SOCIETY OF CHEMISTRY

PAPER

View Article Online
View Journal | View Issue

Cite this: *Nanoscale Adv.*, 2022, **4**, 294

Pyromellitic diamide–diacid bridged mesoporous organosilica nanospheres with controllable morphologies: a novel PMO for the facile and expeditious synthesis of imidazole derivatives†

Ehsan Valiey and Mohammad G. Dekamin *

In this work, novel pyromellitic diamide–diacid bridged mesoporous organosilica (PMAMOS) nanospheres with controllable morphologies and Brønsted acid catalytic centers were designed and prepared through a convenient method by altering the addition sequence of precursors, solvent, and aging time. The obtained PMAMOSs demonstrate high surface areas and uniform pore sizes. FESEM, HRTEM, BET, EDX, XRD, FTIR and TGA analyses were performed to characterize and examine the effective factors for the preparation of PMAMOS nanospheres. Due to the appropriate physicochemical properties including Brønsted acid centers, suitable surface area and thermal stability of the PMAMOS nanosphere material, it was explored in the three-component reaction of benzyl or benzoin, ammonium acetate, and different aldehyde derivatives as a case study of multicomponent reactions. Corresponding imidazole derivatives were obtained in EtOH under reflux conditions in high to quantitative yields and short reaction times. It was also shown that the heterogeneous solid acid can be reused at least five times with negligible loss of its catalytic activity, indicating the appropriate stability and high activity of the newly introduced mesoporous organosilica.

Received 11th October 2021
Accepted 1st November 2021

DOI: 10.1039/d1na00738f

rsc.li/nanoscale-advances

1. Introduction

The design and facile preparation of nanomaterials (NMs) with suitable functional groups, active centres as well as definite morphologies for high-technology applications has received great attention in recent decades. These high-technology NMs can be used in different areas such as catalysis, smart medicine/drug delivery and formulations, sensors and microelectronic devices, gas storage, optical applications, adsorbents, chromatography, *etc.*[1–12] Mesoporous silica materials (MSMs) have received significant attention from both academia and industry as an important class of NMs. The unique features of MSMs include the regular mesoporous structure and tuneable surface properties as well as adjustable pore size, which guarantee their widespread applications in drug delivery, gas storage, heterogeneous catalysis, adsorption, batteries, and optical devices.[3,13–26]

MSMs can be synthesized *via* two general methods: under acidic or alkaline conditions using different templates.[27] Hence, significant efforts have been made to understand their synthesis process in order to control the obtained pore structures and morphologies.[28–33] Indeed, MSMs with excellent mechanical properties, adjustable and appropriate pore volume, high surface area and thermal stability are very appropriate supports for heterogeneous nano-ordered catalytic systems in the synthesis of a large number of fine and bulk chemical products.[34–44]

Periodic mesoporous organosilicas (PMOs) are an important group of hybrid inorganic–organic MSMs that have organosilane bridges in their pore walls.[45–50] The high loading speed, uniform dispersion of organic groups within the framework, different surface characteristics and possibility of anchoring suitable functional groups make PMO materials unique compared to other organosilica materials for different applications.[51–55] Recently, PMOs with different organic bridges and pore sizes as well as porous structures and morphologies have been successfully synthesized.[20,56–64] However, there is still room to design and prepare new PMOs with appropriate physicochemical properties for definite applications including heterogeneous catalysis.

Heterogeneous catalysts play a prominent role in the synthesis of fine chemicals through the multicomponent reaction (MCR) strategy.[65–71] Indeed, imidazole derivatives are an important category of heterocyclic compounds demonstrating biological properties and medicinal applications, which can be prepared using appropriate substrates through the MCR strategy.[32,67,68,72–84] This bunch of 1,3-diazoles exhibits therapeutic behaviors such as antibiotic,[85,86] antifungal,[87,88] and antibacterial activity.[89] Imidazole compounds are used in some medicines

Pharmaceutical and Heterocyclic Compounds Research Laboratory, Department of Chemistry, Iran University of Science and Technology, Iran. E-mail: mdekamin@iust.ac.ir

† Electronic supplementary information (ESI) available. See DOI: 10.1039/d1na00738f

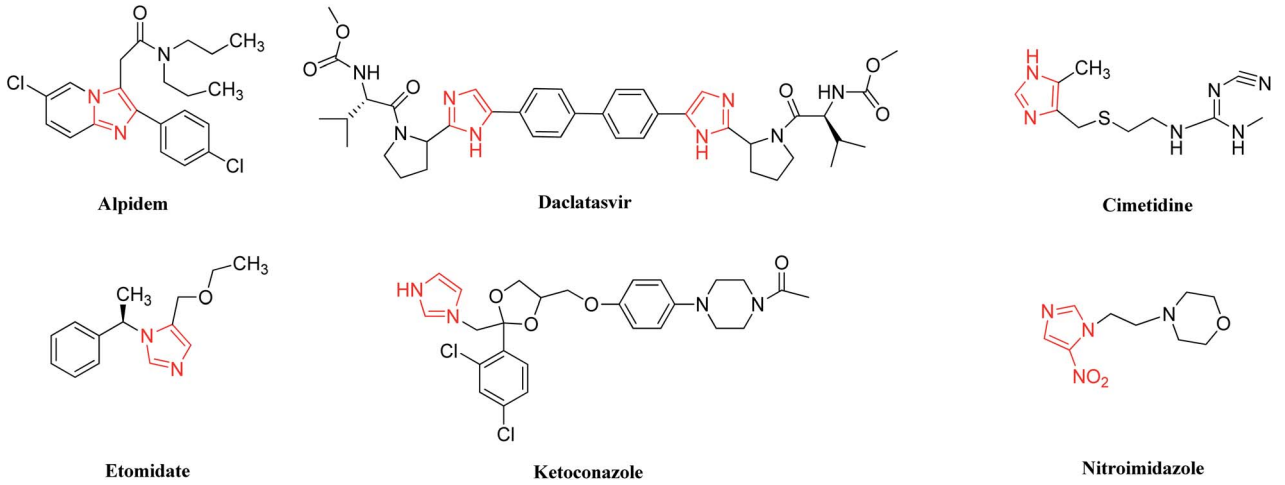

Fig. 1 Examples of medicines containing the imidazole scaffold.

such as the new alpidem,[90–92] cimetidine, etomidate, ketoconazole,[93,94] antiviral daclatasvir[95,96] and nitroimidazole (Fig. 1).

In recent years, the synthesis of imidazole derivatives using benzoin, as a commercially available substrate, in the presence of various catalysts has been reported to a limited extent.[74] Among recent homogeneous or heterogeneous catalysts are molecular iodine,[97] Fe_3O_4/SiO_2-urea nanoparticles,[98] iron–phosphonate nanomaterial,[99] poly(2-acrylamido-2-methylpropanesulfonic acid-

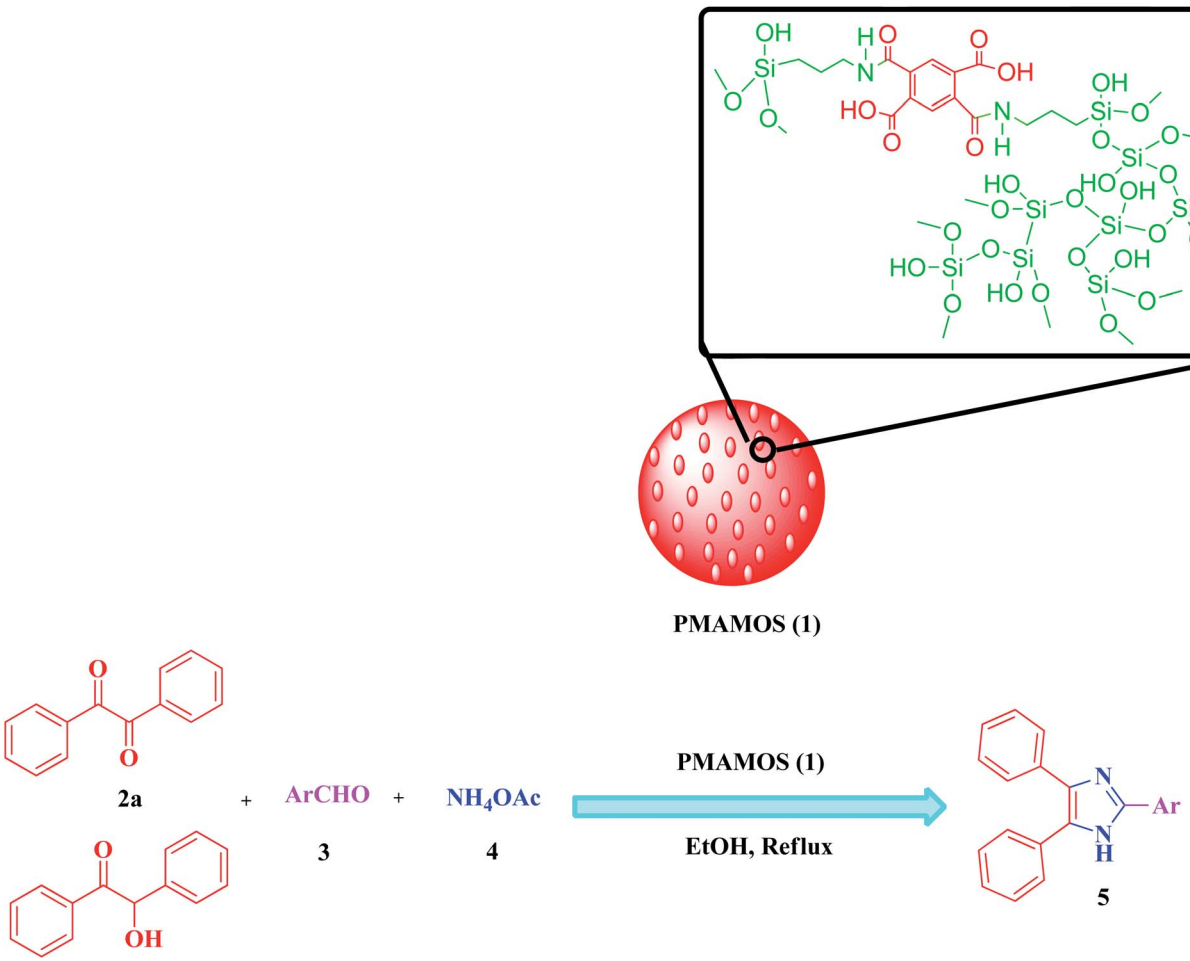

Scheme 1 PMAMOS (1)-catalyzed synthesis of imidazole derivatives through a multicomponent reaction of benzil (2a) or benzoin (2b), aldehyde derivatives (3), and ammonium acetate (4) in EtOH under reflux conditions.

co-acrylic acid-*co*-acrylamide), molecularly imprinted polymer,[100] 2,6-dimethylpyridinium trinitromethanide molten salt,[78] magnetic graphitic carbon nitride,[101] graphene oxide–chitosan composite,[102] ferric(III) nitrate supported on kieselguhr,[103] and isocyanurate-based periodic mesoporous organosilica.[77] In spite of their merits, some of the reported methods for the synthesis of imidazole derivatives suffer from disadvantages due to the high loading of the catalyst, utilizing toxic solvents and/or expensive metal catalysts, low production yields, long reaction times as well as laborious and hard purification procedures and irreversible environmental risks. In continuation of our interest to develop MSMs and especially PMOs for promoting different organic transformations or CO_2 capture,[26,50,55,77,104] herein we wish to report the synthesis of a new pyromellitic diamide–diacid bridged mesoporous organosilica (PMAMOS) with uniform particle size and high purity using a simple, inexpensive and green method. Furthermore, different imidazole derivatives **5** were efficiently synthesized using PMAMOS (**1**), as a solid acid catalyst, under environment-friendly conditions in short reaction times *via* the condensation reaction of benzil (**2a**) or benzoin (**2b**), aldehyde derivatives (**3**), and ammonium acetate (**4**) in EtOH under reflux conditions (Scheme 1).

2. Results and discussion

The pyromellitic diamide–diacid bridged mesoporous organosilica (PMAMOS, **1**) with different morphologies was prepared under green conditions (Scheme 3). The obtained PMAMOS (**1**) samples were then characterized using different techniques such as field emission scanning electron microscopy (FESEM), X-ray powder diffraction (XRD), Brunauer–Emmett–Teller (BET) porosimetry, energy-dispersive X-ray (EDX) spectroscopy, high-resolution transmission electron microscopy (HRTEM), Fourier transform infrared (FTIR) spectroscopy and thermogravimetric analysis (TGA).

In fact, the synthesis of PMOs depends on many factors such as the used template and hydrophobic solutes including mesitylene or CO_2, solvent, temperature, pressure and the synthesis method.[4,5] Therefore, a systematic study should be performed to determine the optimal conditions. In this work, the pyromellitic diamide–diacid (PMDADA) precursor (**I**) was prepared in both THF and DMF at first. Then, the obtained PMDADA precursors (**I**) were used with tetraethyl orthosilicate (TEOS) to afford the novel PMAMOS (**1**) according to known procedures for similar PMOs.[77] Indeed, the PMDADA (**I**) solid powder precursor and

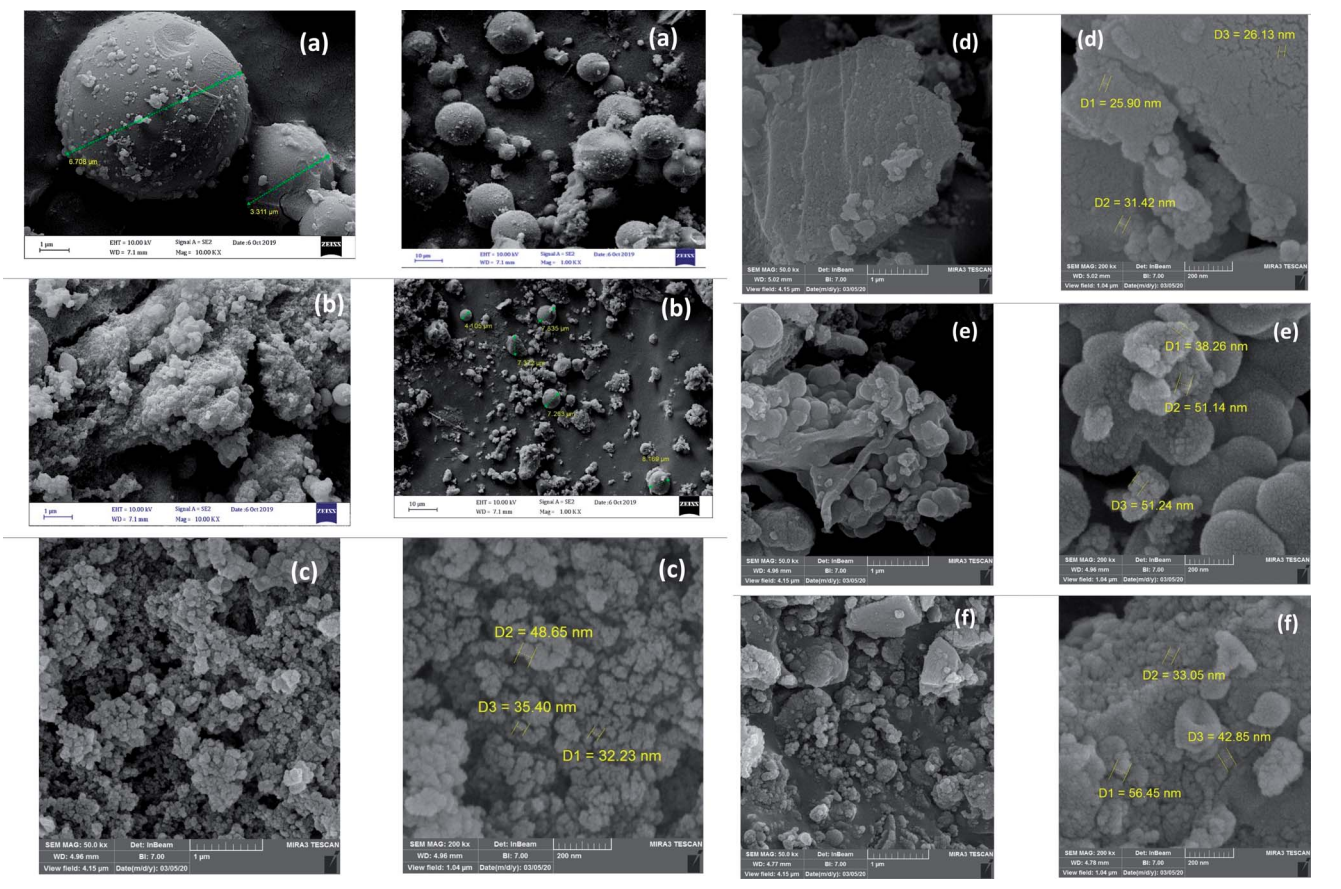

Fig. 2 FESEM images of PMAMOS (**1**) obtained using: precursor **I** prepared in THF (a) or DMF solvent (b) as well as precursor **I** was prepared in THF and subsequently dispersed in acetone (c) with the simultaneous addition of precursor **I** and TEOS to the mixture of HCl and Pluronic P123; PMDADA precursor (**I**) was dissolved in the acidic solution of HCl and Pluronic P123, TEOS was added dropwise later (d); CTAB was dissolved in ammonia solution and used as the template (e); Similar conditions to PMAMOSa but with 48 h aging time (f).

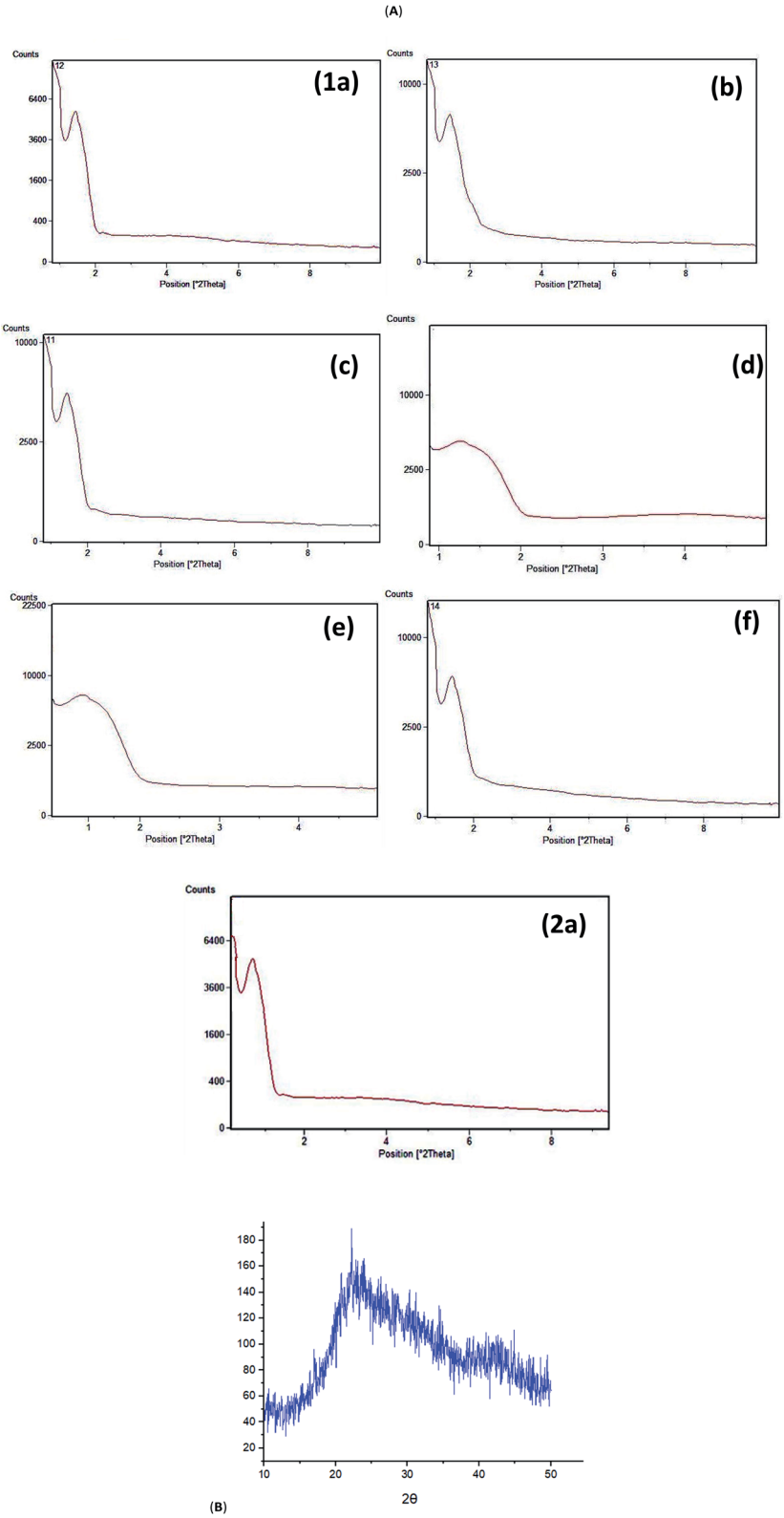

Fig. 3 (A) Low-angle XRD patterns of PMAMOS (**1**) obtained using: precursor **I** prepared in THF (a) or DMF solvent (b) as well as precursor **I** was prepared in THF and subsequently dispersed in acetone (c) with the simultaneous addition of precursor **I** and TEOS to the mixture of HCl and Pluronic P123; PMDADA precursor (**I**) was dissolved in the acidic solution of HCl and Pluronic P123, TEOS was added dropwise later (d); CTAB was dissolved in ammonia solution and used as the template (e); Similar conditions to PMAMOSa but with 48 h aging time; (f) PMAMOSa after five-times recycling (**2a**); (B) Representative wide-angle XRD pattern of PMAMOSa–f (**1**).

TEOS were added simultaneously and step by step to the acidic HCl mixture of Pluronic P123. Fig. 2a shows FESEM images of the obtained PMAMOSa nanospheres after 8 h when THF solvent was used for the preparation of the PMDADA (**I**) precursor (Scheme 3). On the other hand, when DMF was used as the solvent for the preparation of the PMDADA (**I**) precursor, the extent of nanospheres decreased substantially in PMAMOSb (Fig. 2b). Hence, the PMDADA (**I**) precursor was prepared in THF and used in the next experiments for the preparation of relevant PMOs. Since the PMDADA (**I**) precursor is a solid

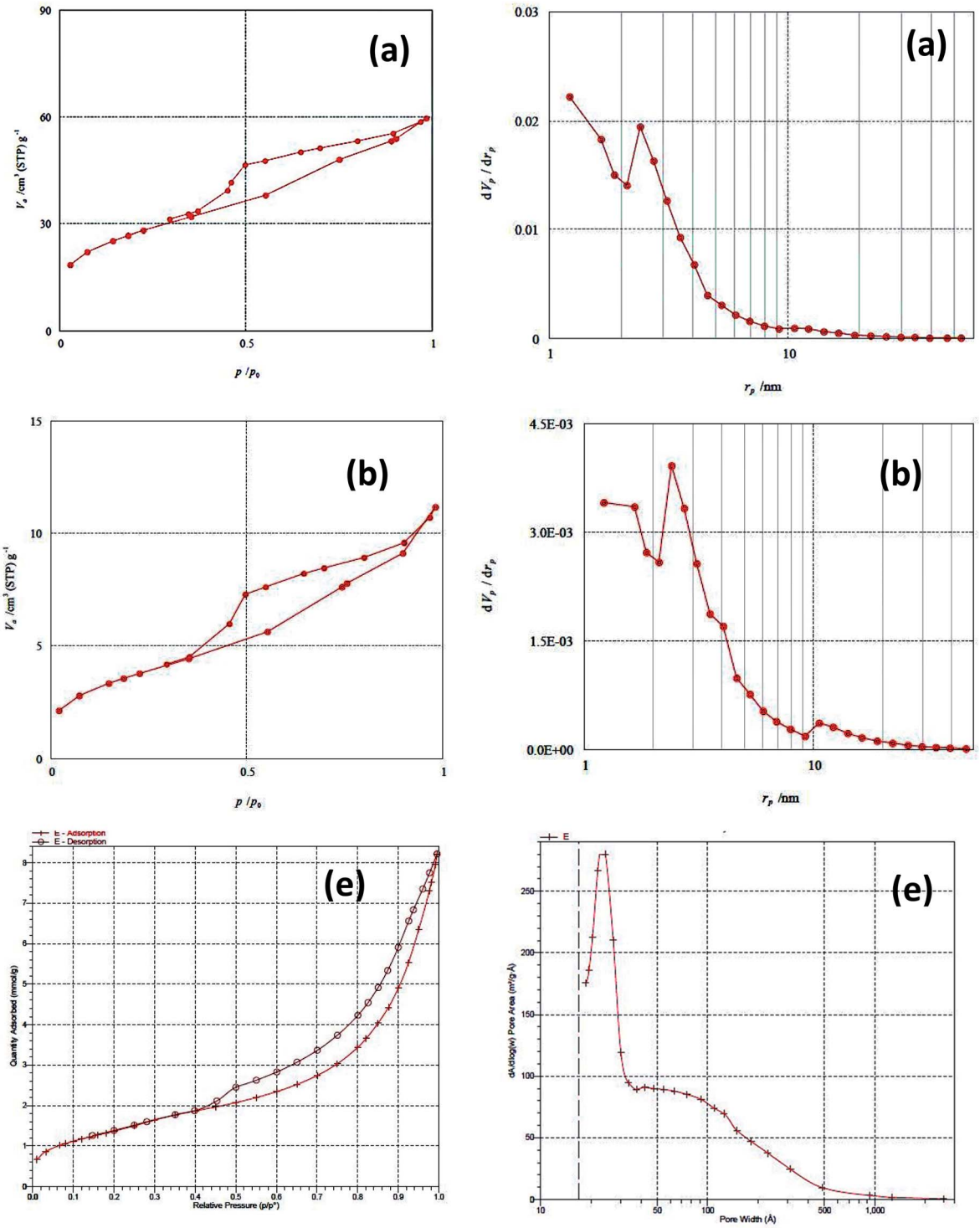

Fig. 4 N_2 adsorption–desorption isotherms of PMAMOSa,b,e (**1**) obtained using the PMDADA precursor **I** prepared in THF (a) or DMF solvent (b) with the simultaneous addition of precursor **I** and TEOS to the mixture of HCl and Pluronic P123. CTAB was dissolved in ammonia solution and used as the template (e).

organic material, it was dispersed in acetone by mechanical stirring in the following experiment. The obtained mixture and TEOS were then added separately and stepwise to the acidic HCl mixture of Pluronic P123 under similar known conditions. Fig. 2c shows FESEM images of the corresponding PMAMOSc. It is obvious that the morphology of the obtained PMO has changed completely. In another experiment, the PMDADA precursor (**I**) was dissolved in an acidic solution of HCl and Pluronic P123 and then TEOS was added dropwise to afford the corresponding PMAMOSd with plate morphology (Fig. 2d). In a further experiment, CTAB was firstly dissolved in ammonia solution, then TEOS and the precursor were added slowly to the obtained mixture. The structure of PMAMOSe formed under these conditions consists of a mixture of plate and spheres (Fig. 2e). In all of the PMAMOSa–e samples, the aging time was 24 h. When an experiment was run under similar conditions to PMAMOSa but with 48 h aging time, the morphology of the obtained PMAMOSf changed completely (Fig. 2f).

In general, mesoporous compounds have two characteristic peaks in their XRD patterns: low-angle peak at $2\theta = 1.1$–1.7° and wide-angle peak at $2\theta = 20$–30°, respectively.[105] XRD patterns of the synthesized structures under different conditions are shown in Fig. 3A. In fact, low angle XRD patterns (Fig. 3a) for PMAMOSa and PMAMOSb structures were observed at $2\theta = 1.22^\circ$ while those of PMAMOSc–f structures appeared at $2\theta = 1.44^\circ$. The wide-angle XRD patterns of all the prepared mesoporous structures are the same, a representative example of them is shown in Fig. 3b.

Fig. 4 shows the N_2 adsorption–desorption isotherms and the corresponding BJH pore-size distribution curves for the PMAMOSa,b,e (**1**) structures synthesized by different methods. They showed type IV isotherms with a H1 hysteresis loop, characteristic of mesoporous materials. As shown, the surface area of PMAMOSb is reduced relative to PMAMOSa, which is probably due to different ratios of the *meta*- and *para*-isomers of the PMDADA precursor (**I**) in DMF compared to THF solvent. The physical properties of the synthesized structures are summarized in Table 1.

The crystal, grain boundaries and surface structure of PMAMOSa,f (**1**) were further examined by high-resolution TEM (HRTEM). The HRTEM image in Fig. 5 shows the single nanocrystalline structure of PMAMOSa,f (**1**).

As shown in Fig. 6a, the EDX analysis of PMAMOSa (**1**) confirmed the presence of Si (8.70%), C (20.93%), O (58.50%) and N (11.87%). On the other hand, Fig. 6b shows the presence of Si (12.73%), C (18.72%), O (59.63%) and N (8.92%) elements in the EDX analysis of PMAMOSb (**1**). Comparison of these two EDX spectra again indicates that the structure of PMAMOSa (**1**) is superior to that of PMAMOSb (**1**) because of the higher concentration of nitrogen in its structure which is a good proof for more incorporation of the PMDADA precursor (**I**) into the texture of the sample.

In the next step, the obtained PMAMOSa–f (**1**) samples were analyzed by FTIR spectroscopy. Fig. 7a shows the FTIR spectra of PMDADA. The band at 3600–2400 cm^{-1} is related to the stretching vibrations of acidic OH groups, and the absorption bands at 1700 and 1652 cm^{-1} can be attributed to the carbonyl acidic groups and amide, respectively. The absorption band in the range of 1564–1470 cm^{-1} corresponds to the C=C stretching of the aromatic ring. Furthermore, Fig. 7b shows the FTIR spectra of PMAMOS (**1**). Interestingly, all PMAMOSa–f (**1**) samples showed similar FTIR spectra. The absorption band at 3600–2400 cm^{-1} is related to the acidic OH groups. On the other hand, the absorption band at 3406 cm^{-1} can be attributed to the NH stretching vibrations. Also, the absorption band at 1716 cm^{-1} belongs to the acidic carbonyl groups whereas the band at 1623 cm^{-1} can be assigned to the amide functional group in the structure of PMAMOS. Moreover, the absorption bands at 1508 cm^{-1} are assigned to the C=C groups and the absorption bands in the range of 1213–1050 cm^{-1} can be attributed to the Si–O–Si and Si–OH groups. Furthermore, the back titration method was used to determine the acidity of different PMAMOS (**1**). In fact, the pH of the PMAMOSa sample was calculated to be 2.15. Also, the pH of PMAMOSb,e samples was calculated using a similar method, which were 2.68 and 3.2 for b and e, respectively.

TGA analysis was also performed to investigate the thermal stability of PMAMOS (**1**) in the range of 50 °C to 800 °C. The TGA curve of PMAMOSa (**1**) in Fig. 8 shows three distinct weight losses. The first two losses at 50–159 °C (9%) and 200–340 °C (32%) are due to the evaporation of surface solvent molecules adsorbed on PMAMOSa (**1**) and thermal decomposition of the organic components of PMAMOS (**1**), respectively. The third weight loss (19%) occurred in the range of 340–500 °C, which can be related to the condensation of silanol groups. These results confirm the successful synthesis of PMAMOSa (**1**).

Table 1 Structural parameters of PMAMOS (**1**) determined from nitrogen sorption experiments

Sample	S_{BET}[a]/$m^2\ g^{-1}$	V_p[b]/$cm^3\ g^{-1}$	D_p[c]/nm	W_t[d]/nm
a	160	0.253	0.992	112.383
b	65	0.017	5.253	7.914
e	130	0.92	3.773	94.019

[a] Specific surface area calculated by the BET method. [b] Total pore volume registered at $P/P_0 = 0.985$. [c] Pore size diameter calculated by the BJH method. [d] Wall thickness calculated as $W_t = a_0 - D_p$.

2.1. Optimization of the reaction conditions for synthesis of imidazoles using PMAMOSa (1) catalyst

In the next step, PMAMOSa (**1**) was applied for the synthesis of imidazole derivatives. For this purpose, the condensation was carried out between benzil (**2a**, 1 mmol), aldehyde (**3**, 1 mmol), and ammonium acetate (**4**, 2.5 mmol) as the model reaction. Initially, in the absence of the catalyst, various conditions including solvent-free conditions as well as water or EtOH at room temperature, 50 °C, or reflux conditions were investigated (Table 2, entries 1–6). As shown in Table 2, in the absence of a catalyst, the reaction yields after 5 h were trace. Interestingly, it was observed that with 5 mg loading of PMAMOSa (**1**) the desired product **5a** was formed in 32–83% yields (Table 2, entries 7–11).

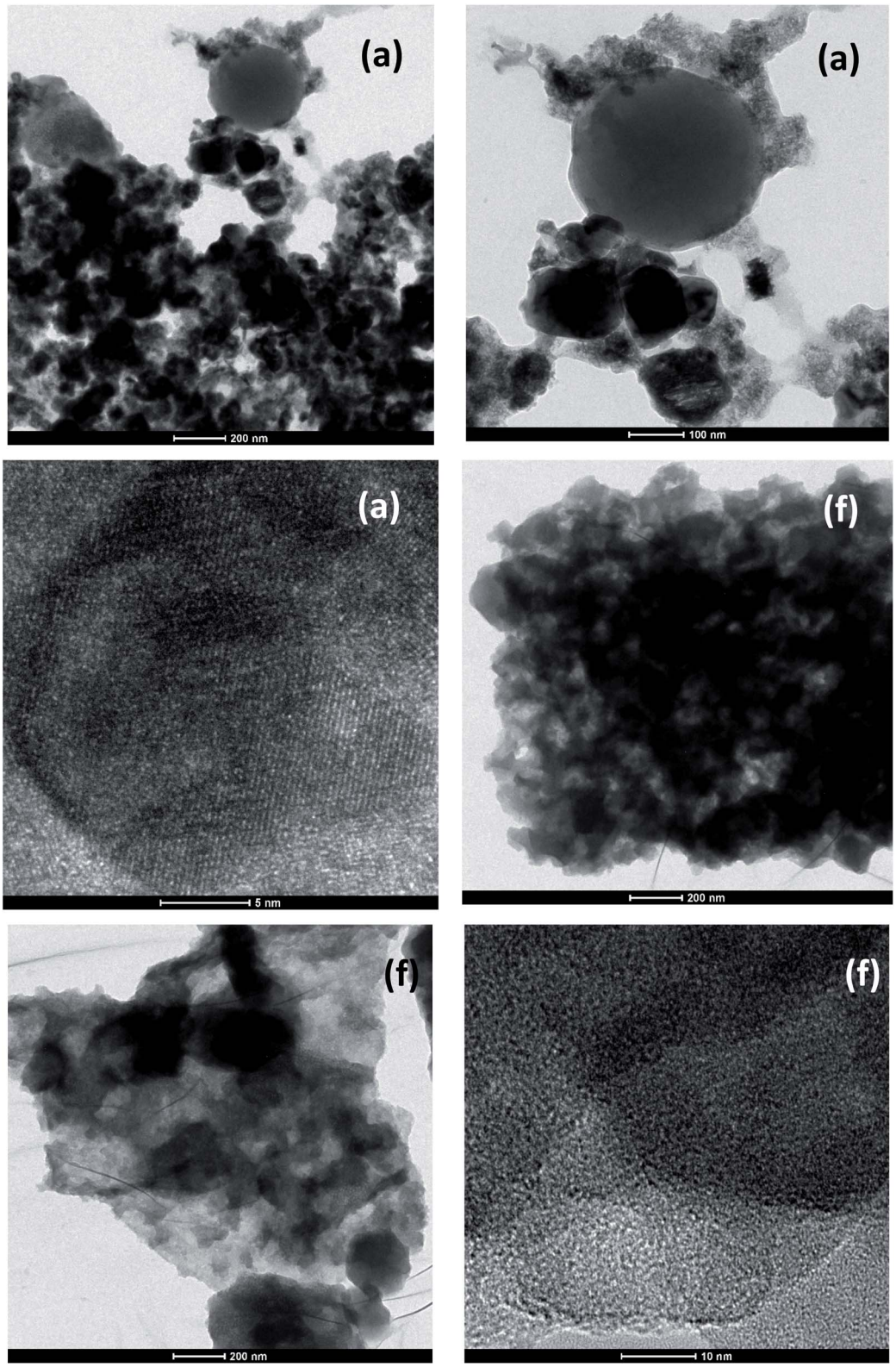

Fig. 5 HRTEM image of PMAMOSa,f (**1**) obtained using the precursor **I** prepared in THF (a) and similar conditions to PMAMOSa but with 48 h aging time (f).

The model reaction yield in EtOH at room temperature reached 32% after 5 h (Table 2, entry 7). The model reaction was also performed in EtOH at 50 °C for 4 h with a yield of 54% as well as under ultrasonic conditions at 60 °C for 3 h with a yield of 68% (Table 2, entries 8 and 9). In EtOH under reflux conditions using 5 mg PMAMOSa (**1**) loading, a remarkable yield of

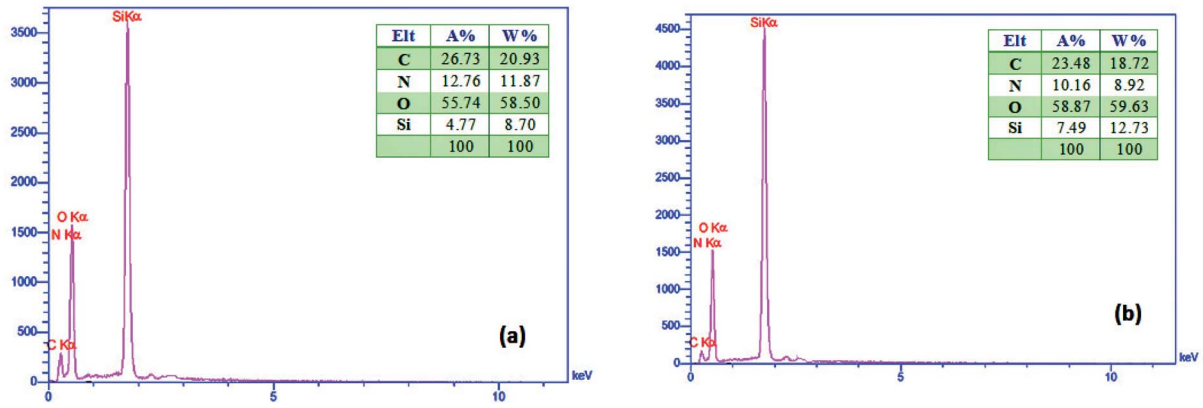

Fig. 6 EDX spectra of the obtained PMAMOS using precursor **I** prepared in THF (a) and DMF solvents (b).

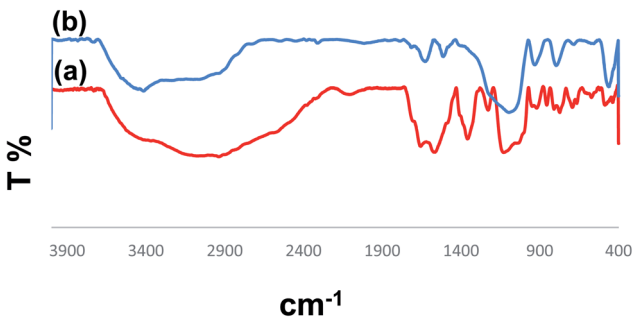

Fig. 7 FTIR spectra of PMDADA (a) and PMAMOSa–f (**1**, b).

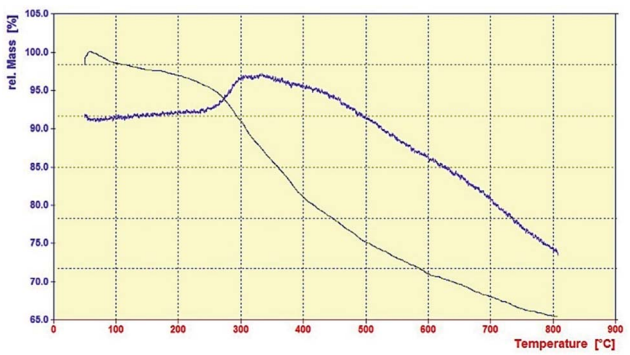

Fig. 8 TGA and DTA curves for PMAMOSa (**1**).

83% was obtained after 2 h (Table 2, entry 10). Despite the positive performance of the EtOH in the model reaction, a yield of 28% was obtained in H_2O under reflux conditions (Table 2, entry 11). Consequently, according to the results summarized in Table 2, EtOH under reflux conditions was used as the optimal solvent for the subsequent experiments. It was also observed that the amount of catalyst has an important role in the reaction rate and yield. For this purpose, the model reaction was investigated under optimal conditions of EtOH under reflux in the presence of 3, 8, 10, and 15 mg of the PMAMOSa (**1**) catalyst (Table 2, entries 12–15). Therefore, 15 mg of the PMAMOSa (**1**) catalyst loading and EtOH under reflux conditions were determined as the optimal conditions for the synthesis of different imidazole derivatives.

In order to extend the application of PMAMOSa (**1**), the three-component condensation of benzil (**2a**) or benzoin (**2b**), aldehyde derivatives (**3a–j**), and ammonium acetate (**4**) was performed under optimal conditions for the synthesis of 2,4,5-trisubstituted imidazole derivatives **5**. The results are summarized in Table 3.

2.2. The proposed mechanism for the synthesis of imidazole derivatives in the presence of PMAMOSa (1)

As shown in the proposed mechanism in Scheme 2, PMAMOSa (**1**) has a mild Brønsted acidic characteristic. Thus, it activates the carbonyl group[109] in aldehyde derivatives **3** through the formation of hydrogen bonding for the nucleophilic addition of ammonium acetate (**4**) to create an intermediate aminal (**I**).[110] In the next step, this intermediate reacts with benzil (**2a**) or benzoin (**2b**) to form intermediates **II** and **II′**, respectively. Oxidation of the intermediate **II′** in the presence of air is facilitated by the anomeric effect of the adjacent *N*-atoms of benzyl C–H bond (path **B**)[78] to afford the cyclic intermediate (**III**) similar to path **A**. Finally, thermal [1,5] H-shift of the intermediate (**III**) produces imidazole derivatives **5** as the final product. Interestingly, the by-products of both **A** and **B** paths are respectively two and three molecules of H_2O, which is good evidence for the environmental benignity of the method. On the other hand, these water molecules are readily sorbed on the surface of catalyst **1** to promote the reaction more efficiently.

One of the advantages of PMAMOSa (**1**) is that it can be easily separated from the reaction mixture and reused in subsequent reactions. To investigate the reusability of the catalyst, PMAMOSa (**1**) was collected after the reaction by filtration, washed with acetone and distilled water, and then dried in an oven at 60 °C. The recovered catalyst was again used in the model reaction at the same time for the previous run. This process was repeated five times without noticeable decrease in the catalytic efficiency of PMAMOSa (**1**, Fig. 9).

To evaluate the efficiency of PMAMOSa (**1**) catalyst, a comparison has been made with the previously reported methods for the synthesis of imidazoles. As shown in Table 4, synthesis of 2,4,5-

Table 2 Optimization of the model reaction conditions for the three-component condensation of benzil (**2a**), 4-chlorobenzaldehyde (**3a**), and ammonium acetate (**4**) in the presence of PMAMOSa (**1**)[a]

Entry	Conditions	Catalyst	Catalyst loading (mg)	Time (min)	Yield (%)
1	Solvent-free/r.t	—	—	300	Trace
2	H_2O/r.t	—	—	300	Trace
3	EtOH/r.t	—	—	300	Trace
4	EtOH/50 °C	—	—	300	Trace
5	EtOH/reflux	—	—	300	20
6	H_2O/reflux	—	—	300	Trace
7	EtOH/r.t	PMAMOSa (**1**)	5	300	32
8	EtOH/50 °C	PMAMOSa (**1**)	5	240	54
9	EtOH/ultrasonic bath/60 °C	PMAMOSa (**1**)	5	180	68
10	EtOH/reflux	PMAMOSa (**1**)	5	120	83
11	H_2O/reflux	PMAMOSa (**1**)	5	120	28
12	EtOH/reflux	PMAMOSa (**1**)	3	120	70
13	EtOH/reflux	PMAMOSa (**1**)	8	120	78
14	EtOH/reflux	PMAMOSa (**1**)	10	90	86
15	**EtOH/reflux**	**PMAMOSa (1)**	**15**	**40**	**98**

[a] Reaction conditions: benzil (**2a**, 1 mmol), 4-chlorobenzaldehyde (**3b**, 1 mmol), ammonium acetate (**4**, 2.5 mmol), and PMAMOS (**1**) unless otherwise noted.

Table 3 Synthesis of imidazole derivatives **5a–j** by the three-component condensation of benzil (**2a**) or benzoin (**2b**), aldehyde derivatives **3a–j**, and ammonium acetate (**4**) in the presence of PMAMOSa (**1**)[a]

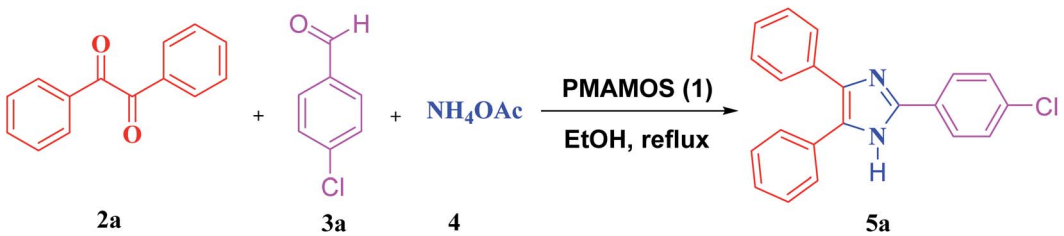

Entry	Aldehyde	Product	Time (min)		Yield (%)		Melting point (°C)	
			Benzil (**2a**)	Benzoin (**2b**)	Benzil (**2a**)	Benzoin (**2b**)	Observed	Reported
1	4-Chlorobenzaldehyde (**3a**)	**5a**	45	40	95	98	261–260	260–262 (ref. 106)
2	2-Chlorobenzaldehyde (**3b**)	**5b**	55	50	85	90	198–196	196–198 (ref. 107)
3	2,4-Dichlorobenzaldehyde(**3c**)	**5c**	60	56	88	92	178–177	177–178 (ref. 107)
4	4-Nitrobenzaldehyde (**3d**)	**5d**	75	65	78	84	201–199	200–202 (ref. 114)
5	3-Nitrobenzaldehyde (**3e**)	**5e**	83	90	70	75	301–298	301–302 (ref. 107)
6	Benzaldehyde (**3f**)	**5f**	80	75	80	86	274–272	272–273 (ref. 108)
7	4-Methoxybenzaldehyde (**3g**)	**5g**	95	90	85	88	229–228	227–228 (ref. 107)
8	Furan-2-carbaldehyde (**3h**)	**5h**	85	80	80	85	201–199	198–200 (ref. 106)
9	2-Thiophenecarboxaldehyde (**3i**)	**5i**	90	83	75	79	261–263	261–263 (ref. 108)
10	4-(Dimethylamino)benzaldehyde (**3j**)	**5j**	120	115	75	85	255–257	256–258 (ref. 108)

[a] Reaction conditions: benzil or benzoin (**2a** or **2b**, 1 mmol), aldehyde derivatives (**3a–j**, 1 mmol) and ammonium acetate (**4**, 2.5 mmol) in the presence of 15 mg PMAMOS (**1**) in EtOH under reflux conditions.

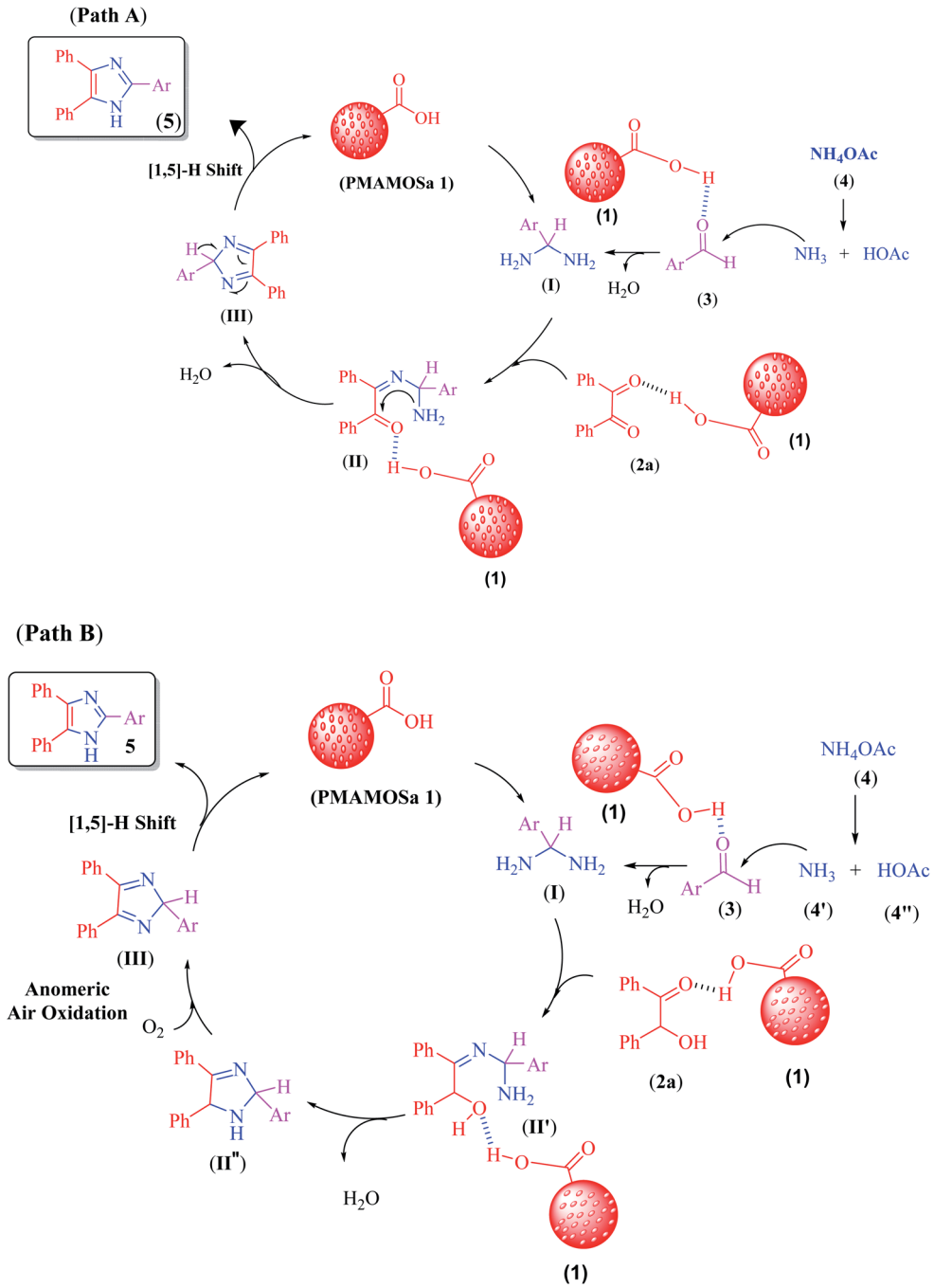

Scheme 2 The proposed mechanism for the synthesis of imidazole derivatives using benzil or benzoin in the presence of PMAMOSa (1) catalyst.

trisubstituted imidazole derivatives in the presence of PMAMOSa (1) has advantages over other methods, such as shorter reaction time, lower catalyst loading, and more environment friendly (green) reaction conditions.

3. Experimental

3.1. Materials and instrumentation

All chemicals were purchased from Merck or Aldrich with high purity and utilized as received without further purification, except for benzaldehyde which was used as a fresh distilled sample. The characterization of PMAMOSa–f (1) was performed by FESEM (TESCAN-MIRA3), EDX (Numerix DXP-X10P), HRTEM (FEI TECNAI F20), FTIR (Shimadzu 8400s), BET (ASAP 2020 micrometrics), and TGA (Bahr Company STA 504). XRD patterns were obtained using a TW 1800 diffractometer with Cu Kα radiation ($\lambda = 1.54050$ Å). All products were characterized by FTIR and ^{1}H NMR spectroscopy using a 500 MHz, Bruker DRX-500 Avance spectrometer in DMSO as compared with those obtained from authentic samples or reported in the literature. Distilled water was used in all experiments.

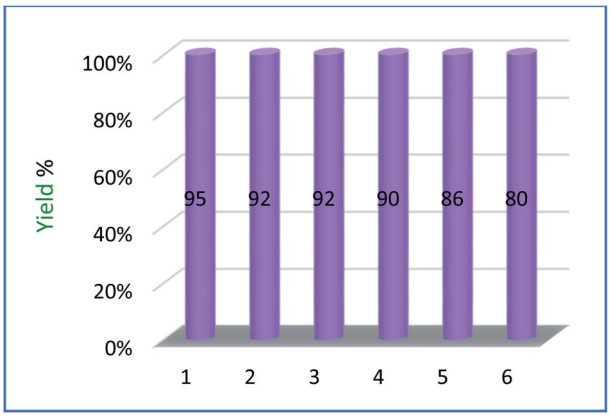

Fig. 9 Reusability of the heterogeneous catalyst PMAMOSa (**1**) in the model reaction to afford **5a**.

3.2. General procedure for the preparation of mesoporous organosilica (PMAMOS, 1)

The PMDADA precursor (**I**) was synthesized using two methods:

In the first method, in a 100 mL round bottom flask, (3-aminopropyl) triethoxysilane (3-APTS, 4 mmol, $d = 0.946$ g mL^{-1}), and 1 mmol of pyromellitic dianhydride (PMDA) were added ito dry THF (15 mL) at 60 °C for 8 h. In the second method, the reaction mixture was dispersed in dry DMF (15 mL) at 80 °C for 8 h. The reaction mixture was then cooled to room temperature. Following this, Et_2O (5 mL) and *n*-hexane (5 mL) were added to the obtained mixture; the obtained white solid was filtered off and washed with Et_2O, then dried in a vacuum oven at 60 °C for 24 h (Scheme 3). The synthesis of the pyromellitic diacid–diamide (PMDADA, **I**) precursor in dry THF was selected as the optimal method according to the results obtained from the characterization data of the obtained PMAMOS. In the next step, Pluronic P123 (4.0 g) was added to a mixture of H_2O (15 mL) and HCl solution (2 M, 150 mL), and stirred at room temperature for 4 h. The obtained mixture was then stirred at 40 °C for 6 h. Next, the precursor (**I**, 3.5 g) and TEOS (38 mmol, 8.5 mL) were slowly added and stirred at 40 °C for 24 h. The reaction temperature was then increased to 100 °C and kept at this temperature for 24 h without stirring. Next, the obtained solid was filtered off, washed, and then dried in an oven at 100 °C for 12 h. Finally, the product obtained in acidic medium was treated under Soxhlet extraction conditions using EtOH for 72 h to afford PMAMOSa,b (**1**). The second step was also done in four different parallel ways: (i) The precursor **I** was first dispersed in acetone and then slowly added with TEOS to the mixture of HCl (2 M) and H_2O, and stirred for 24 h. Following this, the aging time for the mixture was set for 24 h; (ii) The precursor (**I**) was first dissolved in the acidic mixture of HCl (2 M) and H_2O and then TEOS was added to the mixture, and stirred for 24 h. Then, the aging time for the mixture was set for 24 h; (iii) CTAB was dissolved in ammonia solution, then the precursor (**I**) and TEOS were added to the mixture and stirred for 24 h. Then, the aging time for the mixture was set for 24 h; (iv) TEOS and the synthesized precursor (**I**) were added to the mixture simultaneously and stirred for 24 h. Then, the aging time for the mixture was set for 48 h. Hence, other PMAMOSc–f (**1**) structures with different morphologies were obtained, respectively (Scheme 3).

3.3. Measurement of the acidity of PMAMOS using the back titration method

Back titration method was used to determine the acidity of PMAMOSa,b,e samples. Hence, distilled water (35.0 mL), NaCl (0.5 g), PMAMOSa (0.5 g), and aqueous NaOH (10.0 mL, 0.1 M) were added into a beaker and stirred at room temperature for 24 h. Then, a few drops of phenolphthalein (as the indicator) were added, and the excess amount of OH^- ions was titrated with HCl (0.1 M), until the color changed from pink to colorless. Finally, the pH of PMAMOSa was calculated (pH = 2.15). Also, the pH of PMAMOSb,e samples was calculated using the mentioned method, which were 2.68 and 3.2 for b and e, respectively.

3.4. General procedure for the synthesis of 2,4,5-trisubstituted imidazole derivatives 3a–j

In a 5 mL flask, a mixture of benzil (**2a**, 1 mmol) or benzoin (**2b**, 1 mmol), aldehyde (**3**, 1 mmol), ammonium acetate (**4**, 2.5 mmol), and 15 mg of PMAMOSa (**1**) in EtOH (4 mL) was stirred under reflux conditions. The progress of the reaction was monitored by TLC in a mixture of *n*-hexane and EtOAc (3 : 1 v/v). After completion of the reaction, PMAMOSa (**1**) was separated by filtration from the reaction mixture during crystallization of the desired products **3a–j** from EtOH, and was used in next runs.

3.5. Spectral characterization of compounds 5a and 5b

3.5.1 2-(4-Chlorophenyl)-4,5-diphenyl-1*H*-imidazole (5a). Mp: 260–263 °C; IR (KBr, cm^{-1}): 3749, 3419, 1630, 1486, 1436,

Table 4 Comparison of the results obtained for the synthesis of imidazole with benzoin (**2b**) in the presence of PMAMOSa (**1**) and other catalysts

Entry	Catalyst	Conditions and catalyst loading	Time (min)	Yield (%)	Ref.
1	Choline chloride and oxalic acid	Solvent-Free, 60 °C, 0.6 mL	60	90	111
2	Zirconium chloride	CH_3CN, r.t, 46.7 mg	600	93[a]	112
3	Ferric(III) nitrate supported on kieselguhr	Solvent-free, 120 °C, 160 mol%	60	89[a]	103
4	L-Proline	MeOH, 60 °C, 15 mol%	540	88[a]	113
5	PMAMOSa (**1**)	EtOH, reflux, 15 mg	45	95	This work

[a] Benzil (**2a**) was used as the substrate.

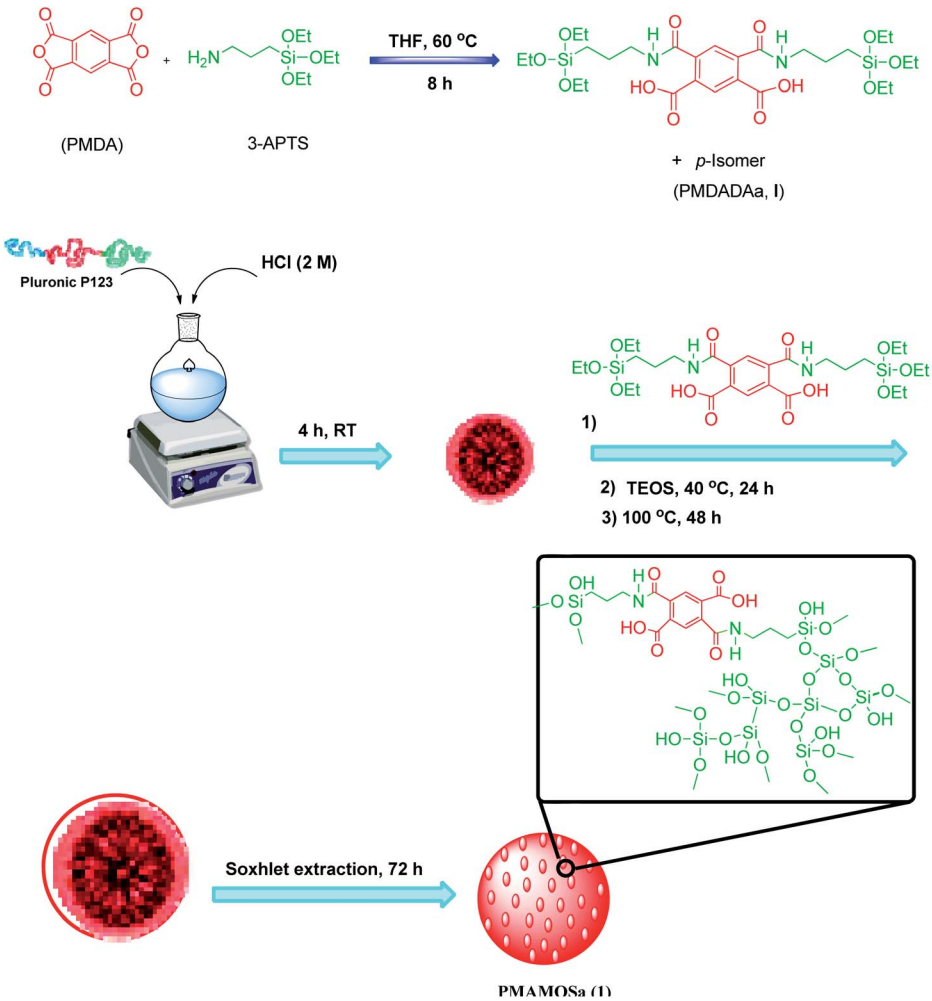

Scheme 3 Schematic preparation steps of PMAMOS (**1**).

1368, 1092, 972, 830, 766, 709, 695; ^{1}H NMR (500 MHz, DMSO-d_6): δ = 7.32–7.85 (m, 13H), 7.87 (s, 1H), 10.30 (br, 1H) ppm; ^{13}C NMR (125 MHz, DMSO-d_6): δ = 127.45, 127.48, 128.05, 128.77, 129.09, 129.57, 129.67, 129.88, 130.51, 130.95, 132.40, 143.24 ppm.

3.5.2 2-(2-Chlorophenyl)-4,5-diphenyl-1*H*-imidazole (5b). Mp: 196–198 °C; IR (KBr, cm^{-1}): 3448, 3059, 1601, 1503, 1478, 1320, 1201, 1070, 761, 693, 605; ^{1}H NMR (500 MHz, DMSO-d_6): δ = 7.29–7.46 (m, 7H), 7.5 (d, 1H, J = 7.7 Hz), 7.66 (d, 4H, J = 7.6 Hz), 8.46 (d, 1H, J = 7.7 Hz), 10.3 (br, 1H) ppm; ^{13}C NMR (125 MHz, DMSO-d_6): δ = 127.48, 127.80, 128.01, 128.79, 129.04, 129.57, 129.67, 129.92, 130.45, 130.89, 132.35, 143.75 ppm.

4. Conclusions

In this study, novel and highly ordered pyromellitic diamide–diacid bridged mesoporous organosilicas (PMAMOSs) with adjustable morphologies and particle sizes were designed and successfully prepared using a convenient method. The obtained PMAMOSs were properly characterized by various spectroscopic, microscopic, adsorption–desorption and analytical methods or techniques. The morphology and pore size were well adjusted by varying the relevant synthesis parameters. Due to the high thermal stability, high surface area (160 m^2 g^{-1}) and uniform pore size (0.992 nm), the new PMAMOSa was used in the three-component condensation reaction of benzil or benzoin, diverse aromatic aldehyde derivatives, and ammonium acetate for the synthesis of 2,4,5-trisubstituted imidazole derivatives under mild conditions as a case study of multicomponent reactions. Appropriate stability and high activity of the newly introduced solid acid, its reusability with a slight decrease in the catalytic activity as well as low cost of preparation and easy isolation of the products can be considered as some of the main advantages of this new synthetic protocol.

Conflicts of interest

There are no conflicts to declare.

Acknowledgements

We are grateful for the financial support from The Research Council of Iran University of Science and Technology (IUST), Tehran, Iran (Grant No. 160/19810). We would also like to

acknowledge the support of Iran Nanotechnology Initiative Council (INIC), Iran.

References

1 P. Sudarsanam, E. Peeters, E. V. Makshina, V. I. Parvulescu and B. F. Sels, *Chem. Soc. Rev.*, 2019, **48**, 2366–2421.
2 C. M. Parlett, K. Wilson and A. F. Lee, *Chem. Soc. Rev.*, 2013, **42**, 3876–3893.
3 B. Kong, C. Selomulya, G. Zheng and D. Zhao, *Chem. Soc. Rev.*, 2015, **44**, 7997–8018.
4 C. Wang, M. Zhang, W. Li, X. Huang, S. Li, S. Luan, X. Hou and Q. Wang, *Soft Matter*, 2017, **13**, 5704–5713.
5 T. Zhao, A. Elzatahry, X. Li and D. Zhao, *Nat. Rev. Mater.*, 2019, **4**, 775–791.
6 J. Jeevanandam, A. Barhoum, Y. S. Chan, A. Dufresne and M. K. Danquah, *Beilstein J. Nanotechnol.*, 2018, **9**, 1050–1074.
7 J. Pandiarajan, in *Nanotechnology Applications in Health and Environmental Sciences*, ed. N. Saglam, F. Korkusuz and R. Prasad, Springer International Publishing, Cham, 2021, pp. 1–28, DOI: 10.1007/978-3-030-64410-9_1.
8 N. Baig, I. Kammakakam and W. Falath, *Mater. Adv.*, 2021, **2**, 1821–1871.
9 G. Gahlawat and A. R. Choudhury, *RSC Adv.*, 2019, **9**, 12944–12967.
10 J. K. Patra, G. Das, L. F. Fraceto, E. V. R. Campos, M. d. P. Rodriguez-Torres, L. S. Acosta-Torres, L. A. Diaz-Torres, R. Grillo, M. K. Swamy, S. Sharma, S. Habtemariam and H.-S. Shin, *J. Nanobiotechnol.*, 2018, **16**, 71.
11 S. Kundu, K. Bramhaiah and S. Bhattacharyya, *Nanoscale Adv.*, 2020, **2**, 5130–5151.
12 M. Ishani, M. G. Dekamin and Z. Alirezvani, *J. Colloid Interface Sci.*, 2018, **521**, 232–241.
13 M. Gao, J. Zeng, K. Liang, D. Zhao and B. Kong, *Adv. Funct. Mater.*, 2020, **30**, 1906950.
14 R. M. Pallares, P. Agbo, X. Liu, D. D. An, S. S. Gauny, S. E. Zeltmann, A. M. Minor and R. J. Abergel, *ACS Appl. Mater. Interfaces*, 2020, **12**, 40078–40084.
15 T. Zhang, B. Huang, A. A. Elzatahry, A. Alghamdi, Q. Yue and Y. Deng, *ACS Appl. Mater. Interfaces*, 2020, **12**, 17901–17908.
16 Y. Zou, B. Huang, L. Cao, Y. Deng and J. Su, *Adv. Mater.*, 2021, **33**, 2005215.
17 A. Yangui, M. Abderrabba and A. Sayari, *J. Taiwan Inst. Chem. Eng.*, 2017, **70**, 111–118.
18 M. G. Dekamin and Z. Mokhtari, *Tetrahedron*, 2012, **68**, 922–930.
19 J. H. Clark, D. J. Macquarrie and S. J. Tavener, *Dalton Trans.*, 2006, 4297–4309.
20 B. Karimi, D. Elhamifar, J. H. Clark and A. J. Hunt, *Chem.–Eur. J.*, 2010, **16**, 8047–8053.
21 P. Hao, B. Peng, B.-Q. Shan, T.-Q. Yang and K. Zhang, *Nanoscale Adv.*, 2020, **2**, 1792–1810.
22 X. Wang, W. Sun, W. Yang, S. Gao, C. Sun and Q. Li, *Nanoscale Adv.*, 2019, **1**, 840–848.
23 T.-Q. Yang, T.-Y. Ning, B. Peng, B.-Q. Shan, Y.-X. Zong, P. Hao, E.-H. Yuan, Q.-M. Chen and K. Zhang, *Catal. Sci. Technol.*, 2019, **9**, 5786–5792.
24 Z. Chen, B. Peng, J.-Q. Xu, X.-C. Xiang, D.-F. Ren, T.-Q. Yang, S.-Y. Ma, K. Zhang and Q.-M. Chen, *Nanoscale*, 2020, **12**, 3657–3662.
25 R. Narayan, U. Y. Nayak, A. M. Raichur and S. Garg, *Pharmaceutics*, 2018, **10**, 118.
26 M. Eslami, M. G. Dekamin, L. Motlagh and A. Maleki, *Green Chem. Lett. Rev.*, 2018, **11**, 36–46.
27 H.-P. Lin, C.-P. Kao, C.-Y. Mou and S.-B. Liu, *J. Phys. Chem. B*, 2000, **104**, 7885–7894.
28 W. C. Yoo and A. Stein, *Chem. Mater.*, 2011, **23**, 1761–1767.
29 Y. Hu, Q. Zhang, J. Goebl, T. Zhang and Y. Yin, *Phys. Chem. Chem. Phys.*, 2010, **12**, 11836–11842.
30 X. Du and J. He, *ACS Appl. Mater. Interfaces*, 2011, **3**, 1269–1276.
31 Z. Gholamzadeh, M. R. Naimi-Jamal and A. Maleki, *C. R. Chim.*, 2014, **17**, 994–1001.
32 E. Ali, M. Naimi-Jamal and M. Dekamin, *Sci. Iran.*, 2013, **20**, 592–597.
33 W. Guo, J.-Y. Park, M.-O. Oh, H.-W. Jeong, W.-J. Cho, I. Kim and C.-S. Ha, *Chem. Mater.*, 2003, **15**, 2295–2298.
34 M. Vallet-Regí, M. Colilla, I. Izquierdo-Barba and M. Manzano, *Molecules*, 2018, **23**, 47.
35 E. Sayed, R. Haj-Ahmad, K. Ruparelia, M. Arshad, M.-W. Chang and Z. Ahmad, *AAPS PharmSciTech*, 2017, **18**, 1507–1525.
36 Y. Alyassin, E. G. Sayed, P. Mehta, K. Ruparelia, M. S. Arshad, M. Rasekh, J. Shepherd, I. Kucuk, P. B. Wilson and N. Singh, *Drug Discovery Today*, 2020, **25**, 1513–1520.
37 N. Nikooei, M. G. Dekamin and E. Valiey, *Res. Chem. Intermed.*, 2020, **46**, 3891–3909.
38 Z. Alirezvani, M. G. Dekamin and E. Valiey, *ACS Omega*, 2019, **4**, 20618–20633.
39 M. Shimizu, K. Michikawa, Y. Maegawa, S. Inagaki and K.-i. Fujita, *ACS Appl. Nano Mater.*, 2020, **3**, 2527–2535.
40 K. Zhang, T. Q. Yang, B. Q. Shan, P. C. Liu, B. Peng, Q. S. Xue, E. H. Yuan, P. Wu, B. Albela and L. Bonneviot, *Chem.–Eur. J.*, 2018, **24**, 478–486.
41 B. Karimi, B. Ghaffari and H. Vali, *J. Colloid Interface Sci.*, 2021, **589**, 474–485.
42 C.-S. Ha and S. S. Park, in *Periodic Mesoporous Organosilicas: Preparation, Properties and Applications*, Springer Singapore, Singapore, 2019, pp. 125–187, DOI: 10.1007/978-981-13-2959-3_5.
43 M. J. Climent, A. Corma and S. Iborra, *Green Chem.*, 2011, **13**, 520–540.
44 Z. Wu, S. Ge, C. Ren, M. Zhang, A. Yip and C. Xu, *Green Chem.*, 2012, **14**, 3336–3343.
45 A. Sayari and S. Hamoudi, *Chem. Mater.*, 2001, **13**, 3151–3168.
46 P. Van Der Voort, D. Esquivel, E. De Canck, F. Goethals, I. Van Driessche and F. J. Romero-Salguero, *Chem. Soc. Rev.*, 2013, **42**, 3913–3955.

47 E. Doustkhah, S. Rostamnia, B. Zeynizadeh, J. Kim, Y. Yamauchi and Y. Ide, *Chem. Lett.*, 2018, **47**, 1243–1245.
48 H. Mekaru, A. Yoshigoe, M. Nakamura, T. Doura and F. Tamanoi, *ACS Appl. Nano Mater.*, 2018, **2**, 479–488.
49 M. Norouzi, D. Elhamifar and S. Abaeezadeh, *Appl. Surf. Sci.*, 2020, **2**, 100039.
50 A. Akbari, M. G. Dekamin, A. Yaghoubi and M. R. Naimi-Jamal, *Sci. Rep.*, 2020, **10**, 10646.
51 A. M. Kaczmarek and P. Van Der Voort, *Materials*, 2020, **13**, 566.
52 A. Corma, D. Das, H. García and A. Leyva, *J. Catal.*, 2005, **229**, 322–331.
53 C. Baleizão, B. Gigante, D. Das, M. Alvaro, H. Garcia and A. Corma, *Chem. Commun.*, 2003, 1860–1861.
54 F. Goethals, I. Ciofi, O. Madia, K. Vanstreels, M. R. Baklanov, C. Detavernier, P. Van Der Voort and I. Van Driessche, *J. Mater. Chem.*, 2012, **22**, 8281–8286.
55 A. Yaghoubi, M. G. Dekamin, E. Arefi and B. Karimi, *J. Colloid Interface Sci.*, 2017, **505**, 956–963.
56 M. Shaker and D. Elhamifar, *Colloids Surf., A*, 2021, **608**, 125603.
57 M. Haghighat, F. Shirini and M. Golshekan, *J. Mol. Struct.*, 2018, **1171**, 168–178.
58 D. Chandra, T. Yokoi, T. Tatsumi and A. Bhaumik, *Chem. Mater.*, 2007, **19**, 5347–5354.
59 S. Das, S. Chatterjee, S. Mondal, A. Modak, B. K. Chandra, S. Das, G. D. Nessim, A. Majee and A. Bhaumik, *Chem. Commun.*, 2020, **56**, 3963–3966.
60 B. Al-Shankiti, W. Al-Maksoud, M. A. H. Muhammed, D. H. Anjum, B. Moosa, J.-M. Basset and N. M. Khashab, *Nanoscale Adv.*, 2020, **2**, 1437–1442.
61 M. I. López, D. Esquivel, C. Jiménez-Sanchidrián, F. J. Romero-Salguero and P. Van Der Voort, *J. Catal.*, 2015, **326**, 139–148.
62 A. M. Kaczmarek, M. Suta, H. Rijckaert, A. Abalymov, I. Van Driessche, A. G. Skirtach, A. Meijerink and P. Van Der Voort, *Adv. Funct. Mater.*, 2020, **30**, 2003101.
63 A. Zebardasti, M. G. Dekamin, E. Doustkhah and M. H. N. Assadi, *Inorg. Chem.*, 2020, **59**, 11223–11227.
64 E. Doustkhah, H. Mohtasham, M. Hasani, Y. Ide, S. Rostamnia, N. Tsunoji and M. H. N. Assadi, *Mol. Catal.*, 2020, **482**, 110676.
65 M. José Climent, A. Corma and S. Iborra, *RSC Adv.*, 2012, **2**, 16–58.
66 S. E. John, S. Gulati and N. Shankaraiah, *Org. Chem. Front.*, 2021, **8**, 4237–4287.
67 F. Sutanto, S. Shaabani, C. G. Neochoritis, T. Zarganes-Tzitzikas, P. Patil, E. Ghonchepour and A. Dömling, *Sci. Adv.*, 2021, **7**, eabd9307.
68 U. K. Sharma, P. Ranjan, E. V. Van der Eycken and S.-L. You, *Chem. Soc. Rev.*, 2020, **49**, 8721–8748.
69 S. Siddiqui and Z. N. Siddiqui, *Nanoscale Adv.*, 2020, **2**, 4639–4651.
70 M. G. Dekamin, M. Azimoshan and L. Ramezani, *Green Chem.*, 2013, **15**, 811–820.
71 A. Yaghoubi, M. G. Dekamin and B. Karimi, *Catal. Lett.*, 2017, **147**, 2656–2663.
72 P. Molina, A. Tárraga and F. Otón, *Org. Biomol. Chem.*, 2012, **10**, 1711–1724.
73 D. A. Shabalin and J. E. Camp, *Org. Biomol. Chem.*, 2020, **18**, 3950–3964.
74 R. Rossi, G. Angelici, G. Casotti, C. Manzini and M. Lessi, *Adv. Synth. Catal.*, 2019, **361**, 2737–2803.
75 O. S. Adeyemi, A. O. Eseola, W. Plass, O. Atolani, T. Sugi, Y. Han, G. E.-s. Batiha, K. Kato, O. J. Awakan and T. D. Olaolu, *Parasitol. Res.*, 2020, 1–17.
76 A. A. Marzouk, A. K. Bass, M. S. Ahmed, A. A. Abdelhamid, Y. A. Elshaier, A. M. Salman and O. M. Aly, *Bioorg. Chem.*, 2020, **101**, 104020.
77 M. G. Dekamin, E. Arefi and A. Yaghoubi, *RSC Adv.*, 2016, **6**, 86982–86988.
78 M. A. Zolfigol, S. Baghery, A. R. Moosavi-Zare and S. M. Vahdat, *RSC Adv.*, 2015, **5**, 32933–32940.
79 S. O. Tomer and H. P. Soni, *Catal. Sci. Technol.*, 2019, **9**, 6517–6531.
80 C. de Graaff, E. Ruijter and R. V. Orru, *Chem. Soc. Rev.*, 2012, **41**, 3969–4009.
81 M. G. Dekamin and M. Eslami, *Green Chem.*, 2014, **16**, 4914–4921.
82 S. Brauch, S. S. van Berkel and B. Westermann, *Chem. Soc. Rev.*, 2013, **42**, 4948–4962.
83 L. Feng, K.-Y. Wang, G. S. Day and H.-C. Zhou, *Chem. Soc. Rev.*, 2019, **48**, 4823–4853.
84 A. Shaabani, A. Rahmati, B. Aghaaliakbari and J. Safaei-Ghomi, *Synth. Commun.*, 2006, **36**, 65–70.
85 M. M. Al Mogren, E. Zerroug, S. Belaidi, A. BenAmor and S. D. A. Al Harbi, *J. King Saud Univ. Sci.*, 2020, **32**, 2301–2310.
86 D. Sharma, B. Narasimhan, P. Kumar, V. Judge, R. Narang, E. De Clercq and J. Balzarini, *Eur. J. Med. Chem.*, 2009, **44**, 2347–2353.
87 S. Bitla, S. R. Sagurthi, R. Dhanavath, M. R. Puchakayala, S. Birudaraju, A. A. Gayatri, V. K. Bhukya and K. R. Atcha, *J. Mol. Struct.*, 2020, **1220**, 128705.
88 a. A. Vijesh, A. M. Isloor, S. Telkar, S. Peethambar, S. Rai and N. Isloor, *Eur. J. Med. Chem.*, 2011, **46**, 3531–3536.
89 R. T. Ulahannan, V. Kannan, V. Vidya and K. Sreekumar, *J. Mol. Struct.*, 2020, **1199**, 127004.
90 Y. Okano, N. Saito-Tarashima, M. Kurosawa, A. Iwabu, M. Ota, T. Watanabe, F. Kato, T. Hishiki, M. Fujimuro and N. Minakawa, *Bioorg. Med. Chem.*, 2019, **27**, 2181–2186.
91 W. Liu, Y. Zhang, J. He, Y. Yu, J. Yuan, X. Ye, Z. Zhang, L. Xue and H. Cao, *J. Org. Chem.*, 2019, **84**, 11348–11358.
92 V. Sankar, P. Karthik, B. Neppolian and B. Sivakumar, *New J. Chem.*, 2020, **44**, 1021–1027.
93 R. Khalifeh and A. Niknam, *Org. Prep. Proced. Int.*, 2020, **52**, 91–98.
94 D. A. Delivanis, A. Sharma, O. Hamidi, M. Shah and I. Bancos, in *Advances in Treatment and Management in Surgical Endocrinology*, Elsevier, 2020, pp. 151–174.
95 A. Rana, B. Mahajan, S. Ghosh, P. Srihari and A. K. Singh, *React. Chem. Eng.*, 2020, **5**, 2109–2114.
96 P. F. Carneiro, B. Gutmann, R. O. de Souza and C. O. Kappe, *ACS Sustainable Chem. Eng.*, 2015, **3**, 3445–3453.

97 D. C. Mungra, H. G. Kathrotiya, N. K. Ladani, M. P. Patel and R. G. Patel, *Chin. Chem. Lett.*, 2012, **23**, 1367–1370.
98 A. Maleki, Z. Alrezvani and S. Maleki, *Catal. Commun.*, 2015, **69**, 29–33.
99 F. Arpanahi and B. Mombeni Goodajdar, *J. Inorg. Organomet. Polym. Mater.*, 2020, 1–10.
100 A. Shaabani, R. Afshari, S. E. Hooshmand and M. Keramati Nejad, *ACS Sustainable Chem. Eng.*, 2017, **5**, 9506–9516.
101 T. S. Ahooie, N. Azizi, I. Yavari and M. M. Hashemi, *J. Iran. Chem. Soc.*, 2018, **15**, 855–862.
102 A. Maleki and R. Paydar, *RSC Adv.*, 2015, **5**, 33177–33184.
103 X. Xu and Y. Li, *Res. Chem. Intermed.*, 2015, **41**, 4169–4176.
104 A. Zebardasti, M. G. Dekamin and E. Doustkhah, *Catalysts*, 2021, **11**, 621.
105 K. Zhang, L.-L. Xu, J.-G. Jiang, N. Calin, K.-F. Lam, S.-J. Zhang, H.-H. Wu, G.-D. Wu, B. l. Albela and L. Bonneviot, *J. Am. Chem. Soc.*, 2013, **135**, 2427–2430.
106 S. S. Nayak, G. C. Wadhawa, V. S. Shivankar, D. D. Patil, M. C. Sonawale and N. A. Mirgane, *Mater. Today: Proc.*, 2020, **37**, 2490–2494.
107 S. A. Dake, M. B. Khedkar, G. S. Irmale, S. J. Ukalgaonkar, V. V. Thorat, S. A. Shintre and R. P. Pawar, *Synth. Commun.*, 2012, **42**, 1509–1520.
108 S. Adhikary, L. Majumder, S. Pakrashy, R. Srinath, K. Mukherjee, C. Mandal and B. Banerji, *ACS Omega*, 2020, **24**, 14394–14407.
109 M. G. Dekamin, S. Ilkhanizadeh, Z. Latifidoost, H. Daemi, Z. Karimi and M. Barikani, *RSC Adv.*, 2014, **4**, 56658–56664.
110 M. G. Dekamin, Z. Karimi and M. Farahmand, *Catal. Sci. Technol.*, 2012, **2**, 1375–1381.
111 M. Bakavoli, H. Eshghi, M. Rahimizadeh, M. R. Housaindokht, A. Mohammadi and H. Monhemi, *Res. Chem. Intermed.*, 2015, **41**, 3497–3505.
112 G. Sharma, Y. Jyothi and P. S. Lakshmi, *Synth. Commun.*, 2006, **36**, 2991–3000.
113 S. Samai, G. C. Nandi, P. Singh and M. Singh, *Tetrahedron*, 2009, **65**, 10155–10161.
114 M. Kalhor and Z. Zarnegar, *RSC Adv.*, 2019, 19333–19346.